

# Dynamics of pivoted slider bearings

Andrew Wilkinson,<sup>1</sup> Marc Pradas,<sup>1,\*</sup> and Michael Wilkinson<sup>1,†</sup>

<sup>1</sup>*School of Mathematics and Statistics, The Open University, Milton Keynes MK7 6AA, United Kingdom*  
(Dated: December 6, 2023)

We obtain the full equations of motion for a wide, pivoted, slider bearing. These are used to review the choice of the optimal position for the pivot point, to discuss its response to time-dependent sliding velocity, and to determine the stability of the motion. The case of an abrupt acceleration of the slider, which results in a large transient increase of the resistive force, is surprisingly complicated. We also discuss a general *transversion* formula for changing the dependent variables in Stokes flow problems.

## I. INTRODUCTION

Slider bearings are used to reduce friction between two solid objects. A thin film of lubricant viscous fluid between the surfaces allows them to slide over each other with relatively little friction, while the pressure of the fluid allows them to remain separated despite a large load perpendicular to the surfaces [1–3]. Slider bearings occur in various forms: here we consider a simple slider which facilitates linear motion of one flat surface over a fixed, flat base. Similar principles are applicable to thrust bearings, which support a force directed along a rotating axis, and journal bearings, where the force is perpendicular. Slider bearings are important element of mechanical engineering, finding applications in almost all systems which involve large moving parts.

The operation of slider bearings depends upon maintaining the film of lubricant. This can be effected by the sliding surface being at an angle to the fixed plate so that the motion entrains lubricant into the gap. One very effective method to ensure that the plate is at a suitable angle is by using a pivoted slider bearing [4]. This allows the angle  $\theta$  between the two surfaces to vary in response to varying the sliding speed  $v$  of the surface. In this configuration, the slider bearing has a pivot point that carries all the vertical load, as illustrated in figure 1. This system was discussed in the book by Michell [4], but the techniques that were used there were limited to considering steady-state solutions with a constant sliding velocity  $v$ . However, in general both the angle  $\theta$  and the gap at the trailing edge of the slider bearing,  $Z$ , are time-dependent, and we should consider the case where  $v$  has a specified time-dependence. In this paper we obtain and analyse the equations of motion for  $\theta$  and  $Z$  when the slider velocity  $v$  is time-dependent.

In the following, we assume that the length of the slider surface is  $L$ , and that the position of the pivot point is at a distance  $sL$  in front of the trailing edge of the bearing surface (see figure 1). In steady motion, the optimal position  $s$  of the pivot might be taken to be that which minimises the resistive force  $F_x$ , with other variables fixed. This question was addressed in Michell’s book [4]. His results show that the optimal pivot position,  $s^*$ , is independent of  $v$ . Also, the steady-state values of  $\theta$ ,  $Z$  and  $F_x$  are all proportional to  $\sqrt{v}$ , as will be explained in section III.

In our formulation, we introduce convenient dimensionless variables

$$\eta = \frac{\theta L}{Z}, \quad \xi = \frac{Z}{L}, \quad \lambda = \ln \xi \quad (1)$$

which we shall term, respectively, the aspect parameter, the gap parameter, and the logarithmic gap parameter. Because the steady-state values of both  $\theta$  and  $Z$  are proportional to  $\sqrt{v}$ , in the steady state the aspect parameter  $\eta$  approaches an equilibrium value  $\eta_0$  which is independent of  $v$  (and which is, in fact, a function only of the pivot point parameter,  $s$ ). Our results on the steady state are shown to be compatible with those in Michell’s book. In particular, we consider the optimal configuration for a slider bearing operated in the steady state, by minimising the resistance force  $F_x$  at a given value of the speed  $v$ . Our analysis shows that this minimum is achieved at a value of the pivot parameter  $s^* \approx 0.3904$ , with aspect parameter  $\eta_0 \approx 2.0713$ . These values are consistent with values quoted in [4]: see table IV, p. 81 of Michell’s book.

We use our equations of motion to extend the analysis of pivoted slider bearings beyond steady conditions. We make a linear stability analysis, and find that the steady-state solutions investigated by Michell are always stable. This implies that, if the bearing is operating close to its steady-state condition and we make a small change to  $v$ , the bearing will converge to its new equilibrium. The timescale for relaxation is of order  $L/v$ , as might be anticipated

\* marc.pradas@open.ac.uk

† m.wilkinson@open.ac.uk

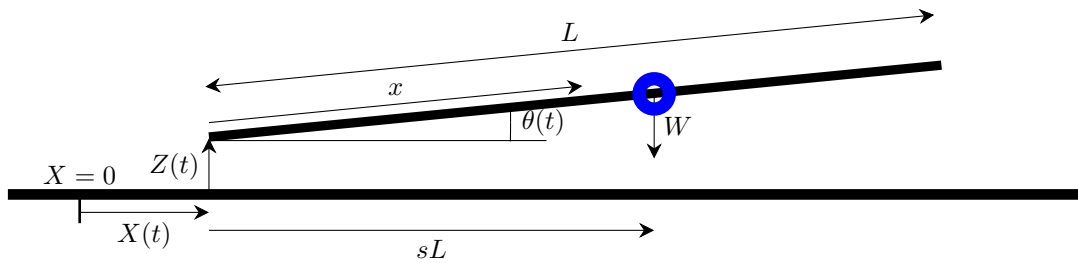


FIG. 1. The slider bearing has length  $L$  and its pivot point (the blue circle) is displaced from the left-hand (trailing) edge by  $sL$ . The bearing is assumed to be sufficiently deep that motion of the fluid in the perpendicular direction to the plane of this diagram can be neglected. The pivot supports a weight per unit depth  $W$ . Motion of the upper element is to the right, with specified speed  $v(t)$ , is opposed by a horizontal viscous drag force per unit depth equal to  $F_x(t)$ . At a time  $t$ , the angle of the plate is  $\theta(t)$ , the gap at the left-hand edge is  $Z(t)$  and the horizontal displacement of the left-hand edge is  $X(t)$ . (Sketch is not to scale).

on physical grounds. The new equilibrium has the same value of  $\eta_0$ , but the value of  $\eta$  is not constant during the transition.

If the slider bearing is abruptly stopped, we show that there is a solution for which the gap parameter decreases as  $\xi \sim t^{-1/2}$ , with a different equilibrium value of  $\eta$ , denoted by  $\eta_-$ . The value of  $\eta_-$  depends only upon the pivot position,  $s$ . We find that these sinking solutions are not stable when the pivot point is too close to the end of the bearing. In cases where this solution is unstable, we hypothesise that one end of the slider contacts the surface in finite time.

The most technologically significant case of non-steady motion is when the bearing is subject to an abrupt acceleration, because the resistive force will be greatly increased during the transient when the gap parameter  $\xi(t)$  is increasing. We analyse the case where the velocity is increased to a constant value  $v$ , and investigate how  $\eta$  and  $\xi$  evolve towards their new equilibrium values. We find that the dynamics of  $\eta(t)$  and  $\xi(t)$  during this transient are complex. If the equilibrium gap parameter for the increased velocity is much greater than the initial value, we show that the value of  $\eta$  becomes very small before reaching its equilibrium value, and that the duration of the transient is much greater than  $L/v$ . We characterise the effect of the acceleration by estimating the excess energy dissipated,  $\Delta E$ , during acceleration to speed  $v$  from an initial condition characterised by coordinates  $\eta_{\text{in}}, \xi_{\text{in}}$ . If  $F_x(t)$  is the resistive force at time  $t$  after initiating the speed increase, and  $F_x(\infty)$  denotes the equilibrium value of this force, then the excess energy dissipated is

$$\Delta E = \int_0^{\infty} dt [F_x(t) - F_x(\infty)] v(t), \quad (2)$$

which we evaluate as a function of the velocity  $v$ , the initial coordinates  $\xi_{\text{in}}, \eta_{\text{in}}$ , and the pivot position parameter  $s$ .

In an earlier paper [5], we used the Reynolds equations of lubrication theory [6] to determine the equations of motion for a flat plate settling onto a flat, horizontal surface. The system has three degrees of freedom, namely the gap  $Z(t)$ , angle  $\theta(t)$  and horizontal displacement  $X(t)$ . The equations of motion connect a three-dimensional, dimensionless, generalised velocity  $\dot{\mathbf{x}}$  to a dimensionless generalised force vector  $\mathbf{f}$ , via a resistance matrix  $\mathbf{B}$ , i.e., we have  $\mathbf{f} = \mathbf{B}\dot{\mathbf{x}}$ . For the equations of motion for the slider bearing considered in this paper, the same dynamical elements appear, but the independent variables are a mixture of forces and velocities. In section II we discuss a general expression for what we shall term the *transversion* of elements between the independent and dependent components in a linear equation of motion. We use this formula to obtain the equations of motion for the slider bearing.

The rest of the paper is organised as follows. In section III we discuss the steady-state solution considered by Michell, which can be obtained from our general form of the equations of motion. In section IV we discuss the local stability properties of the steady-state solution, showing that these solutions are all stable. We determine the relaxation rates, showing that they are of order  $L/v$ . In section V we consider the settling of the bearing when  $v = 0$ , showing that there are solutions with  $\eta$  approaching a constant,  $\eta_-$ , and with  $\xi \sim t^{-1/2}$ . We show that this solution is only stable when the pivot position is in an interval close to the centre of the plate. Section VI discusses the case where  $v$  is suddenly increased by a large factor, and estimates the excess energy dissipated. Section VII is a brief conclusion and summary.

## II. EQUATIONS OF MOTION

The problem analysed in this paper is sketched in Fig. 1. A slider bearing of length  $L$  has a pivot point located at a distance  $sL$  from the left-hand edge of the bearing. We consider the case where the slider bearing is moving with a specified speed  $v(t)$ . We assume that the slider bearing is immersed in a viscous fluid of viscosity  $\mu$  and constant density  $\rho$ , and we model the motion of the vertical gap  $Z(t)$  between the left-hand edge of the bearing and the lower solid surface, and the angle  $\theta(t)$  between the slider bearing and the horizontal.

The problem sketched in Fig. 1 is described in terms of the same dynamical variables as the problem of a flat plate settling onto a flat horizontal surface under the conditions of lubrication theory. This problem was analysed in [5], where the equations of motion were expressed in dimensionless coordinates,  $\eta = \theta L/Z$ ,  $\xi = Z/L$ ,  $\lambda = \ln \xi$ , and a further dimensionless variable  $\zeta = X/L$ , where  $X$  is the horizontal displacement of the plate. The equations of motion in [5] also introduced a dimensionless time variable. In this work we choose the dimensionless time  $\tilde{t}$ , defined by

$$\tilde{t} = \frac{W}{\mu L} t \quad (3)$$

where  $W$  is the downward force per unit depth on the bearing, see Fig. 1. (In the following, reference to a force is understood to be force per unit depth.) The motion of this system can be described by a generalised velocity vector, with components  $(v, d\lambda/dt, d\eta/dt)$ , which can be related to a generalised force vector,  $(F_x, F_z, G)$ , where  $F_x$  is the horizontal force,  $F_z$  the vertical force, and  $G$  the moment of the vertical force about the trailing edge of the bearing. If the bearing supports a weight  $W$ , then  $F_z = W$  and  $G = WsL$ . It will be convenient to express these vectors in dimensionless form, by using the dimensionless time  $\tilde{t}$  given by Eq. (3) to define a dimensionless velocity vector, and defining a dimensionless force vector by dividing the elements  $F_z$  by  $W/\xi^2$ . Hence, we have the dimensionless generalised force vector  $\mathbf{f}$  and velocity vector  $\dot{\mathbf{x}}$  given by

$$\begin{pmatrix} f_1 \\ f_2 \\ f_3 \end{pmatrix} = \begin{pmatrix} \frac{F_x \xi}{W} \\ \xi^2 \\ \xi^2 s \end{pmatrix}, \quad \begin{pmatrix} \dot{x}_1 \\ \dot{x}_2 \\ \dot{x}_3 \end{pmatrix} = \begin{pmatrix} \frac{d\zeta}{d\tilde{t}} \\ \frac{d\lambda}{d\tilde{t}} \\ \frac{d\eta}{d\tilde{t}} \end{pmatrix}. \quad (4)$$

The generalised force and generalised velocity are linearly related:

$$\mathbf{f} = \mathbf{B}(\eta) \dot{\mathbf{x}} \quad (5)$$

where  $\mathbf{f} = (f_1 \ f_2 \ f_3)^T$ ,  $\dot{\mathbf{x}} = (\dot{x}_1 \ \dot{x}_2 \ \dot{x}_3)^T$ , and the components of the  $3 \times 3$  matrix  $\mathbf{B}$  are given in Appendix A (they were derived in [5], where it was shown that they are functions of  $\eta$ , but are independent of the other coordinates). Linear equations of motion in the form of (5) arise frequently in creeping flow problems. The matrix  $\mathbf{B}$  is often referred to as the *resistance matrix* [7], and correspondingly we might refer to its inverse  $\mathbf{C} = \mathbf{B}^{-1}$  as a *compliance matrix*. The coefficients of  $\mathbf{C}$  are also listed in Appendix A.

In the slider bearing problem, the independent variables are a mixture of forces and velocities. Specifically, we fix two force components, namely the normalised vertical force  $f_2 = \xi^2$  and its moment  $f_3 = \xi^2 s$ , and we also specify one velocity, namely the speed of the slider,  $v$ , by the dimensionless velocity

$$\tilde{v} = \frac{\mu}{W} v. \quad (6)$$

The equation of motion should then yield the velocities  $\dot{x}_2 = d\lambda/d\tilde{t}$  and  $\dot{x}_3 = d\eta/d\tilde{t}$ . We should also expect to be able to calculate the dimensionless drag force,  $f_1 = F_x/W\xi$ .

Therefore, the problem of determining the equation of motion has the following structure. We have a matrix  $\mathbf{C}$  which takes us from  $\mathbf{x} = (x_1, x_2, x_3)$  to  $\mathbf{y} = (y_1, y_2, y_3)$ , i.e.,  $\mathbf{y} = \mathbf{C}\mathbf{x}$ . But instead of knowing  $\mathbf{x}$  and wanting to determine  $\mathbf{y}$ , we actually know  $\mathbf{u} = (y_1, y_2, y_3)$  and want to determine  $\mathbf{v} = (x_1, y_2, y_3)$  by writing  $\mathbf{v} = \mathbf{D}\mathbf{u}$ , where  $\mathbf{D}$  is a  $3 \times 3$  matrix.

By means of a direct and mechanical calculation, the elements of  $\mathbf{D}$  are found to be

$$\mathbf{D} = \frac{1}{C_{11}} \begin{pmatrix} 1 & -C_{12} & -C_{13} \\ C_{21} & C_{11}C_{22} - C_{21}C_{12} & C_{11}C_{23} - C_{21}C_{13} \\ C_{31} & C_{11}C_{32} - C_{31}C_{12} & C_{11}C_{33} - C_{31}C_{13} \end{pmatrix}. \quad (7)$$

(The notion of the *Schur complement* ([8]) helps to simplify and to generalise this calculation.) This re-arrangement of

a linear equation of motion involves exchanging the variables  $x_1$  and  $y_1$  between the set of dependent and independent variables. It should find applications in other areas where there are linear equations of motion. We are not aware that the structure has been given a name. We propose that it could be referred to as a *transversion* of the equations of motion.

We then have the equation of motion in the form

$$\begin{pmatrix} f_1 \\ \dot{x}_2 \\ \dot{x}_3 \end{pmatrix} = \begin{pmatrix} \frac{F_x \xi}{W} \\ \frac{d\lambda}{dt} \\ \frac{d\eta}{dt} \end{pmatrix} = \mathbf{D}(\eta) \begin{pmatrix} \dot{x}_1 \\ f_2 \\ f_3 \end{pmatrix} = \mathbf{D}(\eta) \begin{pmatrix} \tilde{v} \\ \xi^2 \\ \xi^2 s \end{pmatrix}. \quad (8)$$

The second and third rows yield two coupled equations of motion for  $\lambda = \ln \xi$  and  $\eta$ :

$$\begin{aligned} \frac{d\lambda}{dt} &= D_{21}(\eta)\tilde{v} + \xi^2 [D_{22}(\eta) + sD_{23}(\eta)] \\ \frac{d\eta}{dt} &= D_{31}(\eta)\tilde{v} + \xi^2 [D_{32}(\eta) + sD_{33}(\eta)]. \end{aligned} \quad (9)$$

Given the solutions  $\lambda(\tilde{t})$  and  $\eta(\tilde{t})$  we can then determine the horizontal force:

$$F_x = \frac{W}{\xi} (D_{11}(\eta)\tilde{v} + \xi^2 [D_{12}(\eta) + sD_{13}(\eta)]). \quad (10)$$

The full set of coefficients  $D_{ij}$  are listed in Appendix A. Some of these coefficients, in particular  $D_{21}$  and  $D_{31}$ , are given exactly by very simple expressions. The expressions for the coefficients occurring in the equations of motion for  $\eta$  and  $\lambda$  are:

$$\begin{aligned} D_{21} &= \frac{\eta}{2}, & D_{22} + sD_{23} &= -16 + 30s + O(\eta), \\ D_{31} &= -\frac{\eta^2}{2}, & D_{32} + sD_{33} &= 30 - 60s + O(\eta). \end{aligned} \quad (11)$$

The equations of motion (9) do not appear to allow an exact and general analytical solution, but in the following sections we address various cases.

### III. STEADY MOTION

We seek a solution where the value of  $\tilde{v}$  is given, and in which both  $\eta$  and  $\lambda$  are time-independent. Comparing the two equations in (9), the condition for a fixed point is

$$\frac{\tilde{v}}{\xi^2} = h_1(\eta) = h_2(\eta), \quad (12)$$

where

$$h_1(\eta) = -\frac{D_{22}(\eta) + sD_{23}(\eta)}{D_{21}(\eta)}, \quad h_2(\eta) = -\frac{D_{32}(\eta) + sD_{33}(\eta)}{D_{31}(\eta)}. \quad (13)$$

The fixed point value  $\eta_0$ , is therefore independent of  $\tilde{v}$ , and satisfies

$$h_1(\eta_0) = h_2(\eta_0). \quad (14)$$

Equation (14) shows that  $\eta_0$  is a function of  $s$ , and solving this numerically yields the relationship illustrated in Fig. 2. Having determined  $\eta_0$ , the fixed point value of  $\xi$  satisfies

$$\xi_0 = \sqrt{\frac{\mu v}{W h_1(\eta_0)}}. \quad (15)$$

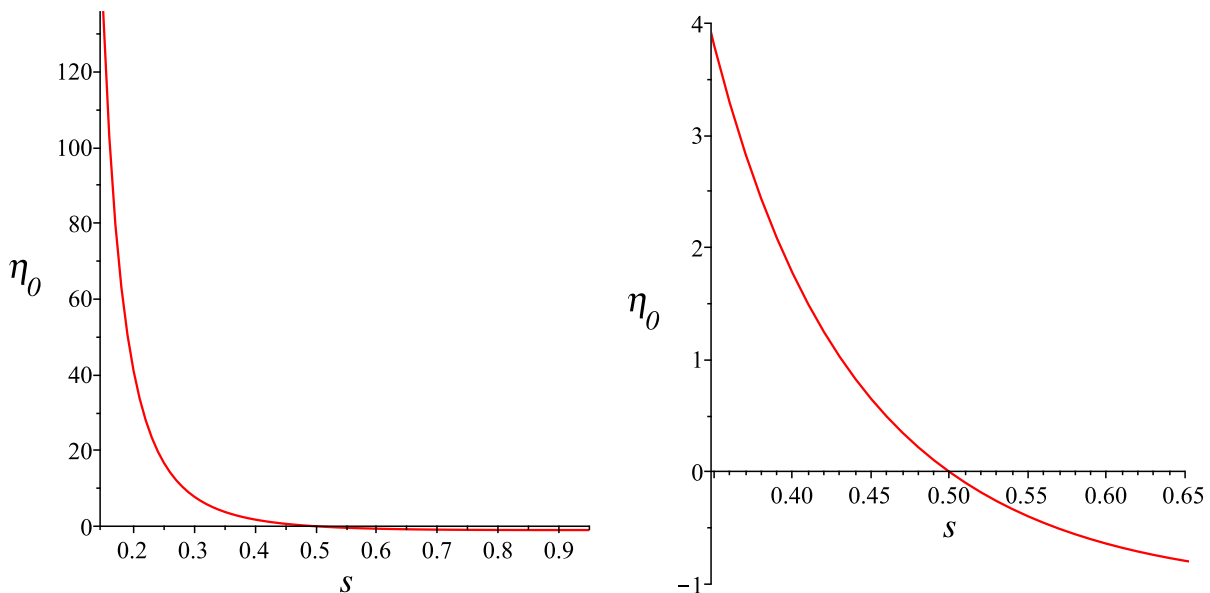


FIG. 2. Plots of the steady-state value of  $\eta$  as a function of the pivot position,  $s$ . The right hand plot shows an expanded view of the area of particular interest.

The horizontal force in the steady state is

$$F_x = W\xi_0 [D_{11}(\eta_0)h_1(\eta_0) + D_{12}(\eta_0) + sD_{13}(\eta_0)] . \quad (16)$$

Note that  $F_x \propto \bar{v}^{1/2}$ , which is different from the usual situation in viscous flow, where force is proportional to velocity. This unusual scaling arises because the angle and the gap of the slider change in order to support the load.

We can also analyse the steady-state solution by starting from equation (5), and considering a solution with  $\dot{\lambda} = \dot{\eta} = 0$ , by setting  $\dot{\mathbf{x}} = (\bar{v}, 0, 0)$ , giving

$$F_x = \frac{\mu}{\xi} B_{11}(\eta_0)v \quad (17a)$$

$$W = \frac{\mu}{\xi^2} B_{21}(\eta_0)v \quad (17b)$$

$$W s L = \frac{\mu L}{\xi^2} B_{31}(\eta_0)v \quad (17c)$$

(these equations also correspond with equations (3.6) of [5]). For given  $s$ , these three equations are to be solved for  $F_x$ ,  $\eta$  and  $\xi$ . Given the solution for  $F_x$ , the bearing performance is optimised by minimising the ratio  $F_x/W$ . Dividing the third equation of (17) by the second gives

$$s(\eta_0) = \frac{B_{31}(\eta_0)}{B_{21}(\eta_0)} = \frac{(-4\eta_0 - 6) \ln(\eta_0 + 1) + \eta_0^2 + 6\eta_0}{2\eta_0 ((\eta_0 + 2) \ln(\eta_0 + 1) - 2\eta_0)} \quad (18)$$

which tells us that a fixed point of  $\eta$  maps to a position along the bearing, which is independent of the load on the bearing and the horizontal velocity. (Here we used expressions for the coefficients  $B_{ij}(\eta)$  given in Appendix A). Solving equation (18) numerically again gives the steady-state value of  $\eta$  as a function of  $s$  illustrated in figure 2, as expected.

The first two equations of (17) lead to

$$F_x = \frac{B_{11}(\eta_0(s))}{\sqrt{B_{21}(\eta_0(s))}} \sqrt{\mu v W} . \quad (19)$$

Figure 3 shows the resistive force as a function of  $s$ , when  $\mu v W = 1$ . The optimum pivot, which minimises the resistive force, is at position  $s^* = 0.3904\dots$ , which is independent of  $\bar{v}$ , and corresponds to  $\eta = \eta_0 = 2.0713\dots$ . The

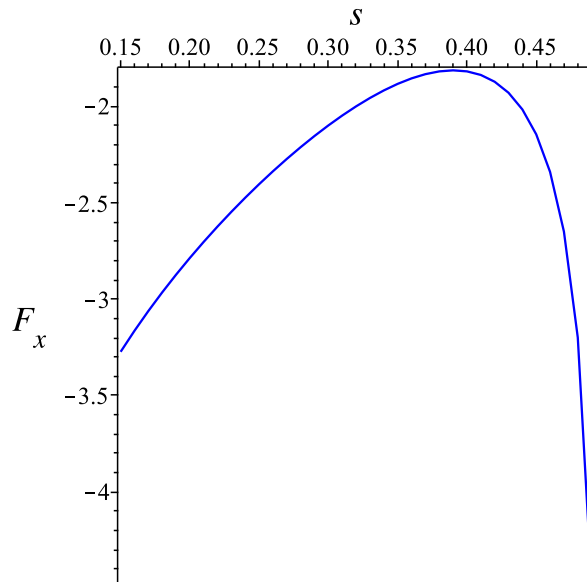


FIG. 3. Plot of  $F_x$  as a function of of the pivot position,  $s$ .

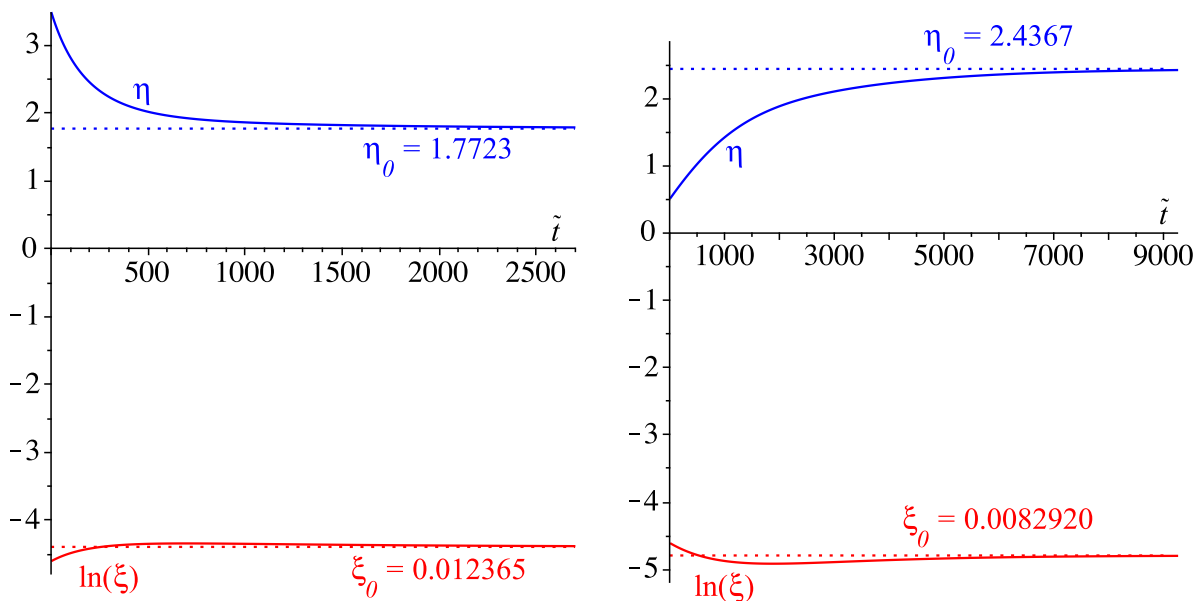


FIG. 4. Plots illustrating relaxation of a pivoted bearing towards its equilibrium configuration when moving with a constant speed. The left panel shows the pivot at  $s = 0.4$  and speed  $\tilde{v} = 0.001$  with initial conditions  $\eta_{\text{in}} = 3.5$ ,  $\xi_{\text{in}} = 0.01$ . The right panel shows the pivot at  $s = 0.38$  and speed  $\tilde{v} = 0.0005$  with initial conditions  $\eta_{\text{in}} = 0.5$ ,  $\xi_{\text{in}} = 0.01$ .

resistive force for this optimal pivot position is  $F_x = -1.8125 \dots \times \sqrt{\mu\nu\bar{W}}$ . We also used Maple to solve equations (8) numerically. Figure 4 illustrates convergence to the steady state solution predicted by (14) and (15).

#### IV. STABILITY OF STEADY FLOW

Figure 4 shows convergence towards the steady-state solutions. In this section, we consider whether the steady-state solutions are stable in the general case.

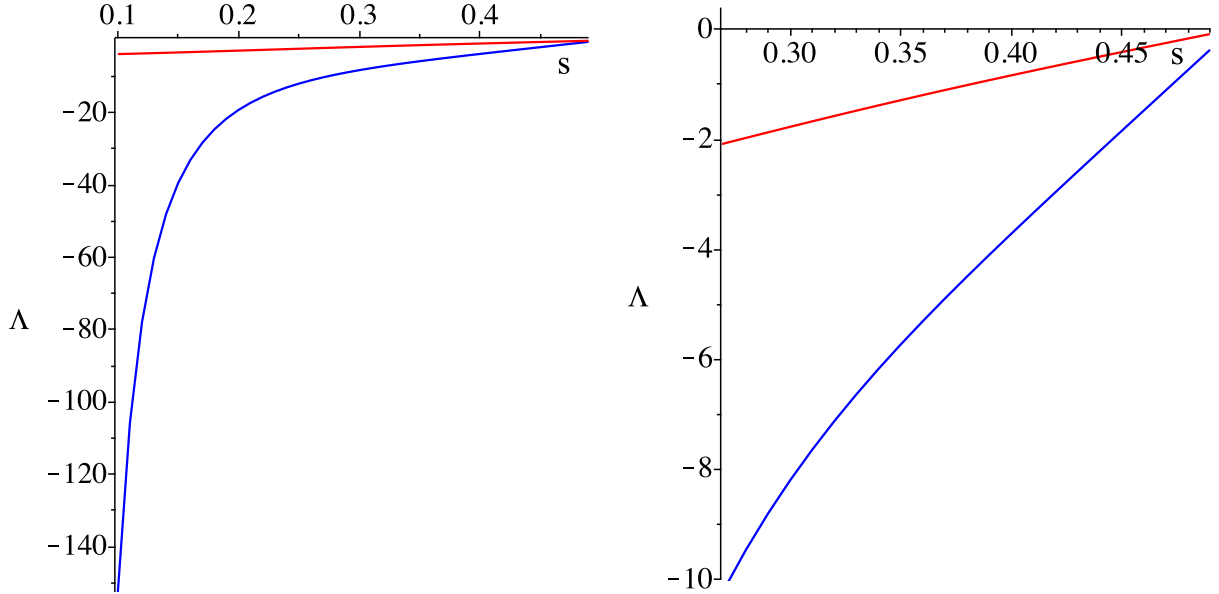


FIG. 5. Plot of the eigenvalues of the matrix  $\mathbf{M}$  as a function of the pivot point position  $s$  (which defines the steady-state aspect parameter  $\eta_0$ ). These define the stability of the steady-state solution. Since they are both negative the steady-state solutions are locally stable. Values calculated at 0.01 intervals from  $s = 0.1$  to  $s = 0.49$ . Right hand panel shows expanded view of the region where both eigenvalues  $> -10$ .

Using (11), the equations of motion (9) can be written in the form

$$\begin{aligned}\frac{d\lambda}{d\tilde{t}} &= \frac{\eta\tilde{v}}{2} + \exp(2\lambda)A(\eta), \\ \frac{d\eta}{d\tilde{t}} &= -\frac{\eta^2\tilde{v}}{2} + \exp(2\lambda)B(\eta).\end{aligned}\quad (20)$$

The steady state conditions give the relations

$$A(\eta_0)\eta_0 = -B(\eta_0), \quad \xi_0^2 = -\eta_0\tilde{v}/2A(\eta_0). \quad (21)$$

Considering small deviations from the steady-state  $\eta(\tilde{t}) = \eta_0 + \delta\eta(\tilde{t})$  and  $\lambda(\tilde{t}) = \lambda_0 + \delta\lambda(\tilde{t})$ , we have

$$\begin{pmatrix} \frac{d\delta\lambda}{d\tilde{t}} \\ \frac{d\delta\eta}{d\tilde{t}} \end{pmatrix} = \tilde{v}\mathbf{M}(\eta_0) \begin{pmatrix} \delta\lambda \\ \delta\eta \end{pmatrix} \quad (22)$$

where

$$\mathbf{M}(\eta) = \begin{pmatrix} -\eta & \frac{1}{2}\left(1 - \frac{\eta A'(\eta)}{A(\eta)}\right) \\ -\frac{\eta B(\eta)}{A(\eta)} & -\eta\left(1 + \frac{B'(\eta)}{2A(\eta)}\right) \end{pmatrix}. \quad (23)$$

The solution of equation (22) may be expressed in terms of the eigenvectors,  $\mathbf{e}_i$  and eigenvalues,  $\Lambda_i$ , of the matrix  $\mathbf{M}$ . In particular, the steady-state solutions are locally stable if the eigenvalues  $\Lambda_i$  are both negative. These eigenvalues are plotted, as a function of  $s$ , in Fig. 5. The fact that the eigenvalues are always negative implies that the steady-state solutions, investigated in [4], are in fact always stable. The timescale for convergence to the equilibrium values,  $\eta_0$ ,  $\xi_0$ , is determined by the inverse of the eigenvalue which is smaller in magnitude. The eigenvalues are proportional to the elements of the matrix  $\mathbf{M}$ , and therefore to  $\tilde{v}$ . This implies that the relaxation in the dimensionless time  $\tilde{t}$  is of order  $1/\tilde{v}$ . In terms of dimensioned quantities, the relaxation time is therefore of order  $L/v$ , which is the timescale for the lubricant film to pass under the bearing, as might be expected on physical grounds. Relaxation

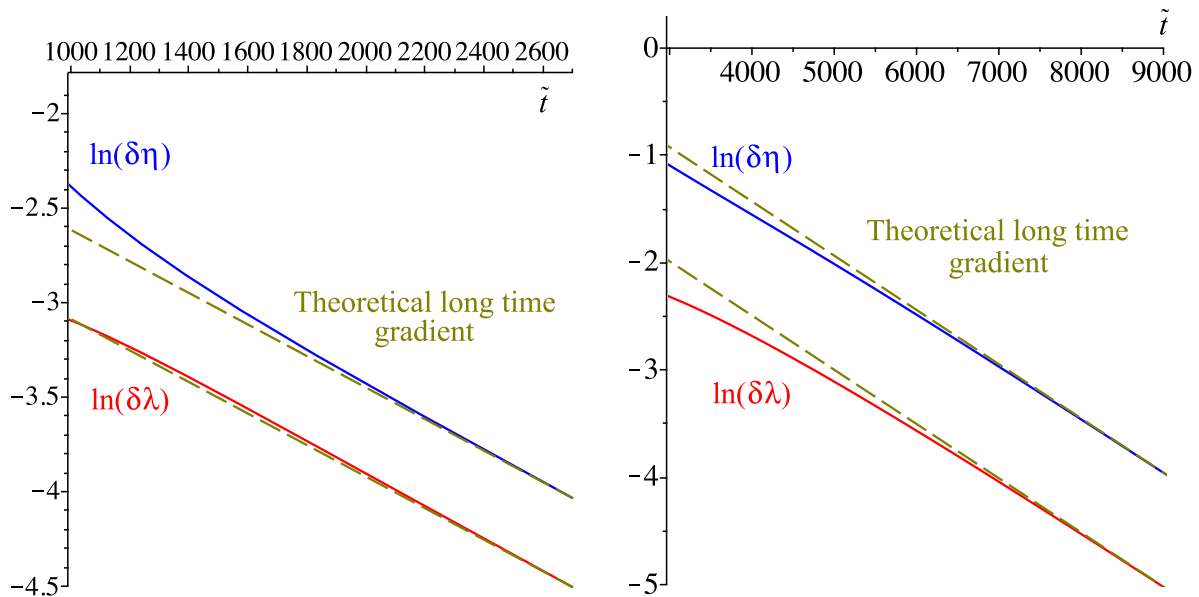


FIG. 6. Plots of  $\ln(\delta\eta)$  and  $\ln(\delta\lambda)$  as they approach their equilibrium values for the situations shown in figure 4, with superimposed (olive) lines showing their theoretical gradients (which are the bearing speed multiplied by the minimum magnitude eigenvalue of the matrix  $\mathbf{M}$ ).

toward the steady-state is illustrated in Fig. 6, for the cases which were treated in Fig. 4. In section VI we show that the equilibration time can be much greater than  $L/v$  when the final velocity is sufficiently large that this perturbative approach is not applicable.

## V. SINKING OF STATIONARY SLIDER

In this section we consider the settling of the bearing when it stops moving, so that  $\tilde{v} = 0$ . Under these conditions, equations (9) give

$$\begin{aligned}\frac{d\xi}{d\tilde{t}} &= \xi^3 [D_{22}(\eta) + sD_{23}(\eta)] \equiv \xi^3 A(\eta), \\ \frac{d\eta}{d\tilde{t}} &= \xi^2 [D_{32}(\eta) + sD_{33}(\eta)] \equiv \xi^2 B(\eta).\end{aligned}\quad (24)$$

If there is a solution of the equation

$$B(\eta_-) = 0, \quad (25)$$

then there is a solution for which the bearing sinks with its aspect parameter  $\eta$  equal to  $\eta_-$ . In the following we obtain  $\xi(\tilde{t})$  for this solution, and investigate the stability of  $\eta$  under a perturbation about its fixed point,  $\eta_-$ .

If  $\eta$  is constant, the first equation of (24) gives

$$\xi^2 = \frac{\xi(0)^2}{1 - 2\xi(0)^2 A(\eta_-)\tilde{t}}, \quad (26)$$

so  $\xi \sim \tilde{t}^{-1/2}$  as  $\tilde{t} \rightarrow \infty$ . If  $\delta\eta$  is a small perturbation about the fixed point  $\eta_-$  satisfying  $B(\eta_-) = 0$ , then

$$\frac{d\delta\eta}{d\tilde{t}} \sim \xi^2 B'(\eta_-)\delta\eta + 2\xi B(\eta_-)\delta\xi = \xi^2 \delta\eta B'(\eta_-). \quad (27)$$



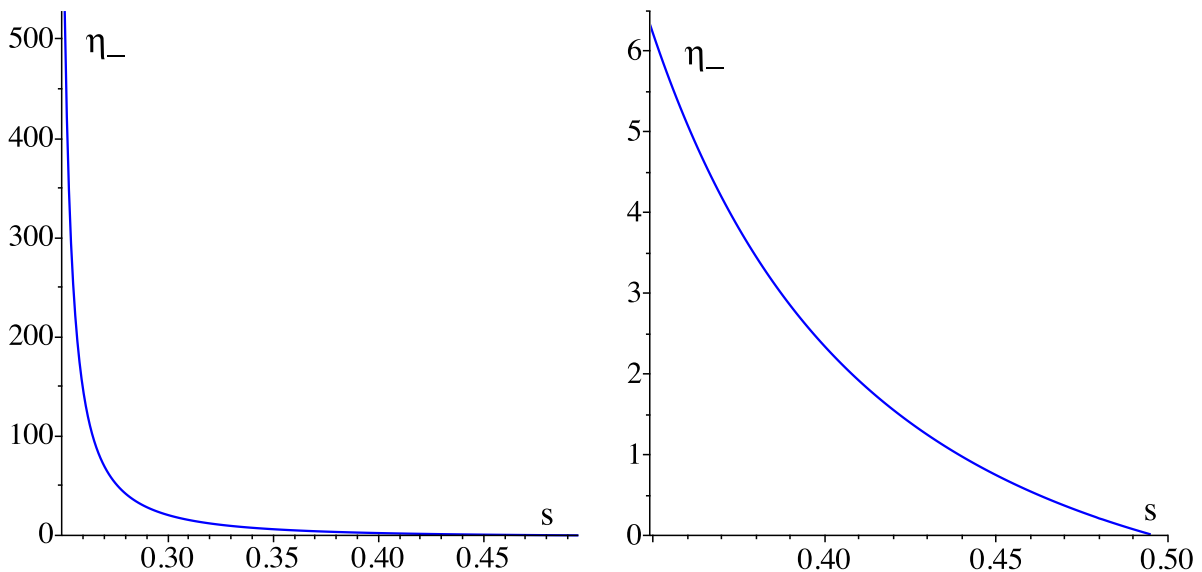


FIG. 7. Plot of the fixed point aspect parameter,  $\eta_-$ , for sinking motion of a stationary slider, as a function of  $s$ . The right hand panel shows expanded view of the region where  $s > 0.35$ .

Combining this with the first equation of (24), we have

$$\frac{d\delta\eta}{d\xi} = \frac{\delta\eta}{\xi} \frac{B'(\eta_-)}{A(\eta_-)}, \quad (28)$$

so,

$$\delta\eta(\tilde{t}) = \delta\eta(0) \left( \frac{\xi(\tilde{t})}{\xi(0)} \right)^{\frac{B'(\eta_-)}{A(\eta_-)}}, \quad (29)$$

and as  $\tilde{t} \rightarrow \infty$ ,  $\xi(\tilde{t}) \rightarrow 0$ , so  $\delta\eta \rightarrow 0$  and the solution is stable if  $B'(\eta_-)/A(\eta_-) > 0$ .

Now let us consider whether a solution satisfying  $B(\eta_-) = 0$  exists, and whether it is stable. Substituting for  $D_{32}$  and  $D_{33}$  (using expressions given in Appendix A), and defining  $\psi = \ln(1 + \eta)$ , leads to an expression of the form

$$B(\eta) = \frac{\eta^4 [2(1 + \eta)\psi + \eta^2(1 - 4s) - 2\eta]}{12(2\psi^2\eta + \psi\eta^2 + 2\psi^2 + 2\psi\eta - 4\eta^2)} \equiv \frac{\eta^4 C(\eta)}{D(\eta)}, \quad (30)$$

which defines functions  $C(\eta)$  and  $D(\eta)$ . Since  $D(\eta) > 0$  for  $\eta > 0$ , the condition  $B(\eta_-) = 0$  is then solved by finding a solution to  $C(\eta_-) = 0$ , or else by  $\eta_- = 0$ . Considering the first of these possibilities, if  $C(\eta_-) = 0$  since we have  $C(0) = 0$  and  $C'(\eta) = 2\ln(1 + \eta) + 2\eta(1 - 4s)$ , then  $C(\eta)$  cannot be 0 for  $\eta > 0$  and  $0 < s \leq \frac{1}{4}$ , so there is no solution to the equation  $B(\eta_-) = 0$  for  $s$  in this range. However, considering  $C(\eta_-) = 0$  for  $\eta > 0$  and  $\frac{1}{4} < s < \frac{1}{2}$ , here  $C'(\eta)$  always has a single zero, corresponding to a maximum of  $C(\eta)$ , which is positioned at  $\eta \rightarrow 0$  as  $s \rightarrow \frac{1}{2}$  from below and at  $\eta \rightarrow \infty$  as  $s \rightarrow \frac{1}{4}$  from above. Hence there is an  $\eta_-$  for which  $C(\eta_-) = 0$  which occurs to the right of the zero of  $C'(\eta)$ , i.e.,  $0 < \eta_- < \infty$ , with  $\eta_- \rightarrow \infty$  as  $s \rightarrow \frac{1}{4}$  from above. Figure 7 illustrates this solution  $\eta_-$  of (25) as a function of  $s$ .

Equation (30) suggests that  $\eta_- = 0$  may be another solution of (25), but  $D(\eta)$  also vanishes as  $\eta \rightarrow 0$ . Application of L'Hospital's rule gives  $B(0) = 30(1 - 2s)$ , so  $\eta_- = 0$  is only a solution for  $s = \frac{1}{2}$ , i.e., the pivot point is in the middle of the slider. This is coincident with the limit of the solution of  $S(\eta) = 0$  as  $s \rightarrow 1/2$ . Equation (29) shows that the solution with constant  $\eta$  is stable provided  $B'(\eta_-)/A(\eta_-)$  is positive. In figure 8 this quantity is plotted as a function of  $s$ , which defines  $\eta_-$ , confirming the solution is stable for  $\frac{1}{4} < s < \frac{1}{2}$ . Figure 9 illustrates examples of this type of motion. For values of  $s \leq \frac{1}{4}$  where there are no real solutions to equation (25), we hypothesise that the bearing would make contact with the plane in finite time.

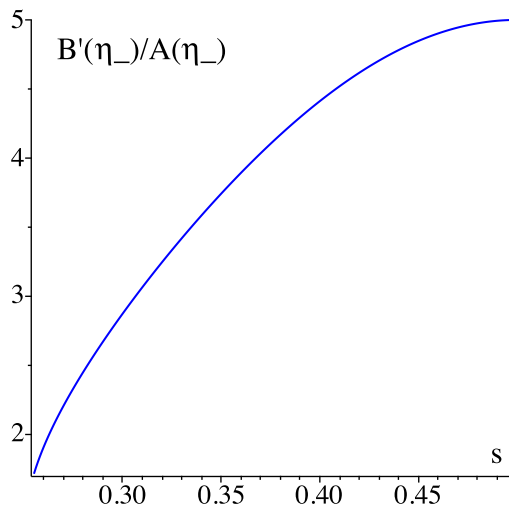


FIG. 8. Plot of  $B'(\eta_-)/A(\eta_-)$  for pivot point values in the interval between  $s = 1/4$  and  $s = 1/2$ .

## VI. RESPONSE TO LARGE INCREASE OF VELOCITY

Let us consider what happens when the coordinates of the slider are initially  $\xi_{\text{in}}$  and  $\eta_{\text{in}}$ , and the velocity  $\tilde{v}$  is suddenly increased to a ‘large’ value, such that the steady state gap  $\xi_0$  satisfies  $\xi_0/\xi_{\text{in}} \gg 1$ . We argue that, when  $\xi_0/\xi_{\text{in}} \gg 1$ , the value of  $\eta$  falls to a very low value,  $\underline{\eta}$ , before increasing to  $\eta_0$ . This behaviour can be observed in Fig. 10. Let us consider why this happens, and how this mechanism leads to a strategy for analysing this transient.

Consider the evolution of  $\lambda(\tilde{t})$  and  $\eta(\tilde{t})$  as described by equations (20), illustrated in figure 10. At the start of the transient, the smallness of  $\xi_{\text{in}}$  ensures that only the terms proportional to  $\tilde{v}$  on the RHS of equations (20) are significant. If the terms proportional to  $\xi^2 = \exp(2\lambda)$  are dropped, the resulting equations are analytically solvable. The solutions of these truncated equations are valid in the initial stage (*phase I*) of the transient, implying that  $\lambda$  increases and  $\eta$  decreases, until we reach a stage, (*phase II*), where the two terms on the RHS of the *second* equation of (20) are comparable. Note that, because the first equation of (20) has a different dependence upon  $\eta$ , the term proportional to  $\exp(2\lambda)$  remains negligible in the first equation of (20) during phase II.

The evolution of  $\lambda$  and  $\eta$  during these first two phases of the transient is, therefore, described by the following truncated approximation of (20):

$$\frac{d\lambda}{d\tilde{t}} = \frac{\tilde{v}}{2}\eta, \quad (31)$$

$$\frac{d\eta}{d\tilde{t}} = -\frac{\tilde{v}}{2}\eta^2 + \exp(2\lambda) [(30 - 60s) + O(\eta)]. \quad (32)$$

The value of  $\eta$  reaches its minimum  $\underline{\eta}$  during phase II, at time  $\tilde{t}$ . At this point, the two terms on the RHS of (32) balance, while  $d\lambda/d\tilde{t}$  is positive. As  $\tilde{t}$  increases, we reach *phase III* of the transient, where the term proportional to  $\exp(2\lambda)$  on the RHS of (32) is dominant, which results in  $\eta$  increasing. In the final, *phase IV*, of the transient,  $\lambda$  becomes sufficiently large that the term which was dropped on the RHS of (31), proportional to  $\exp(2\lambda)$ , becomes significant. In this final phase, the values of  $\xi = \exp(\lambda)$  and  $\eta$  approach the stable fixed point values,  $\xi_0$  and  $\eta_0$ , which corresponds to the velocity  $v$  and pivot position  $s$ .

We are primarily concerned with estimating the energy dissipation during the transient, which is dominated by the initial phases, when  $\xi$  is small. In sub-section VI A we consider the evolution of  $\eta$  and  $\lambda$  during phases I and II, and we make a simple estimate of the values of  $\underline{\eta}$  and  $\tilde{t}$  based upon these solutions. We then (sub-section VI B) use these approximate solutions for  $\eta(\tilde{t})$  and  $\lambda(\tilde{t})$  to estimate the excess energy dissipated.

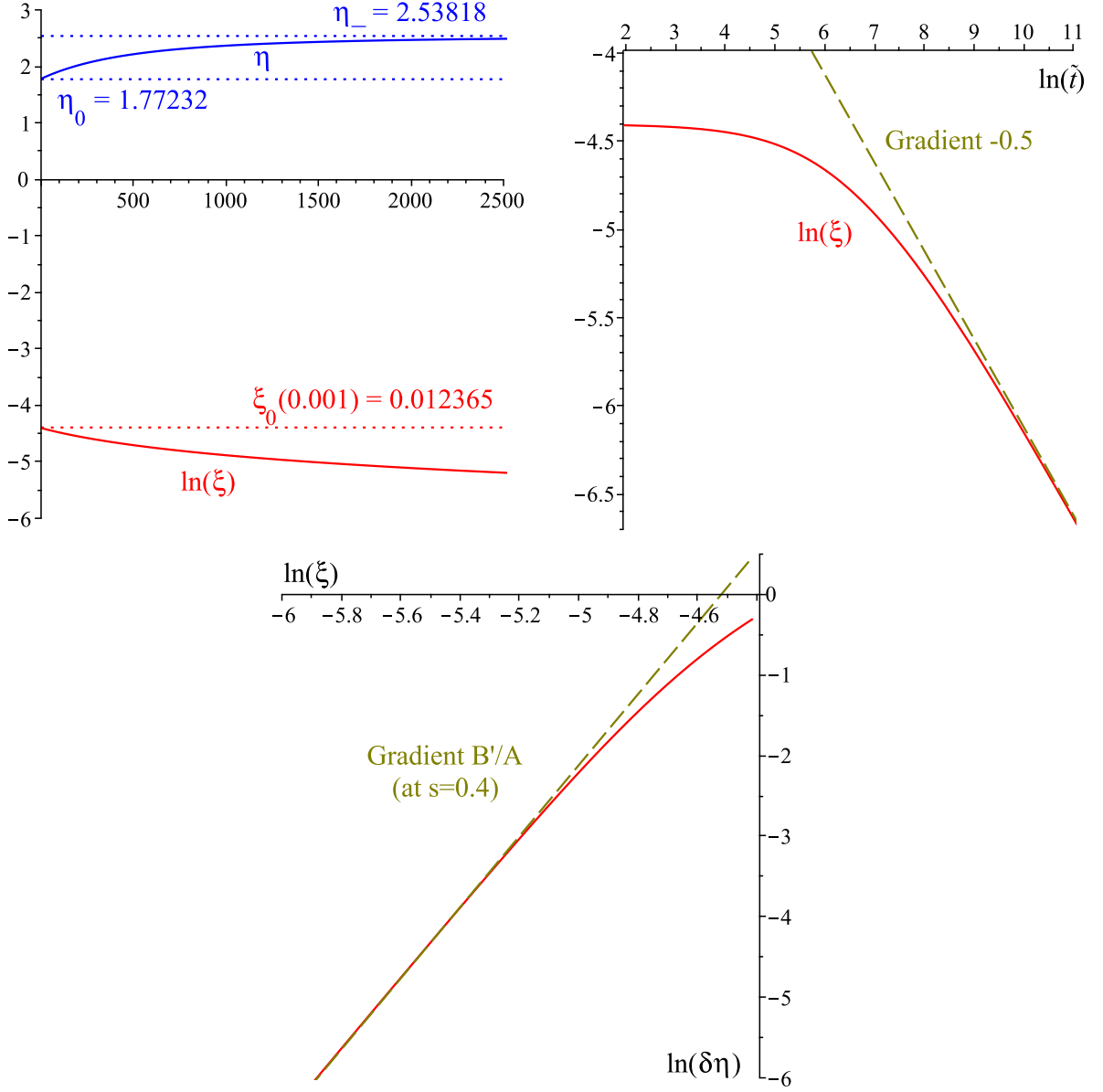


FIG. 9. Plots illustrating the motion of a bearing pivoted at  $s = 0.4$  starting from dynamic equilibrium, then settling after the speed is reduced to zero. Top left-hand panel: initial speed  $v = 0.001$  is suddenly reduced to zero. The value of  $\eta$  changes from  $\eta \approx \eta_0$  to  $\eta \approx \eta_-$ . Top right-hand panel: illustrates that the settling is asymptotic to  $\xi \sim \tilde{t}^{-1/2}$ . Bottom panel illustrates that  $\delta\eta$  is asymptotic to  $[\xi(\tilde{t})]^{\left(\frac{B'(\eta_-)}{A(\eta_-)}\right)}$

### A. Initial phases of the transient

We begin by developing a solution for phase I of the motion (where  $\xi \ll \xi_0$ ), by ignoring  $O(\xi^2)$  terms of equations (31) and (32). The latter gives

$$\frac{d\eta}{d\tilde{t}} = -\frac{1}{2}\eta^2\tilde{v}. \quad (33)$$

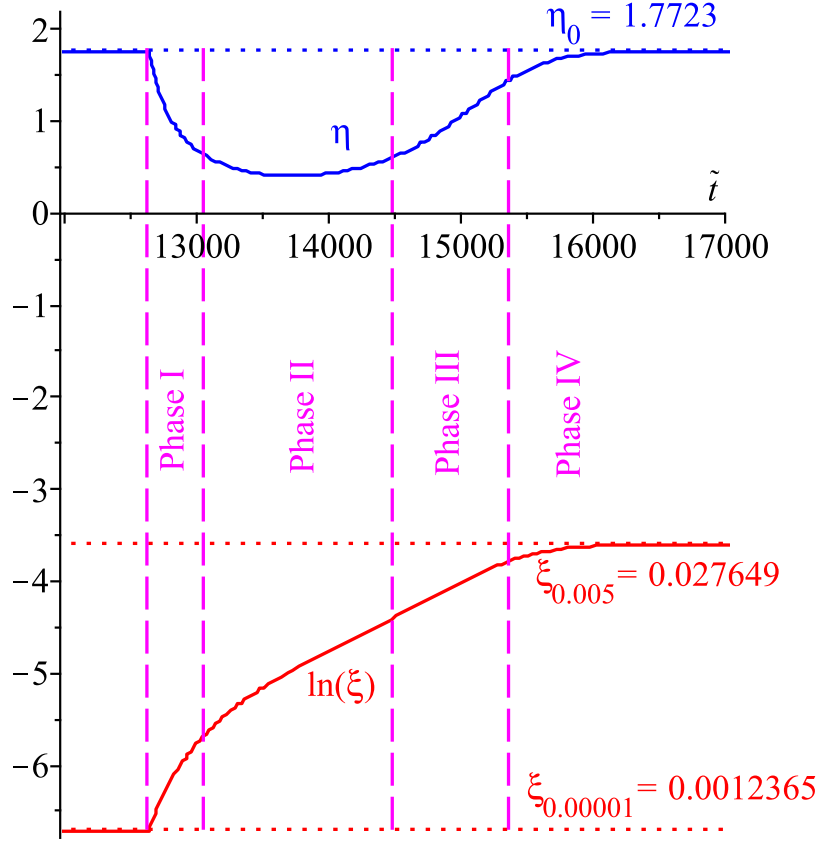


FIG. 10. A bearing pivoted at  $s = 0.4$  is established in its equilibrium configuration when first moving with a constant speed of 0.00001. Its speed is then instantaneously increased by a factor of 500 to 0.005 and it relaxes towards a new equilibrium with  $\eta_0$  unchanged, but a different  $\xi_0$  (shown as  $\xi_{0.00001}$  and  $\xi_{0.005}$ ). The evolution, described by equations (20), can be divided into four phases. In phase I,  $\xi$  is sufficiently small that the terms in  $\exp(2\lambda)$  can be neglected in both equations. In phase II, the two terms on the RHS of the second equation are comparable, but the term in the first equation proportional to  $\exp(2\lambda)$  remains negligible. Later, in phase III, the term proportional to  $\exp(2\lambda)$  dominates the RHS of the second equation, so that  $\eta$  increases. Finally, in phase IV, a new equilibrium is established.

Taking  $\eta = \eta_{\text{in}}$ ,  $\tilde{t} = 0$  at the point of the speed increase, we obtain

$$\eta(\tilde{t}) = \frac{2\eta_{\text{in}}}{2 + \tilde{v}\eta_{\text{in}}\tilde{t}}. \quad (34)$$

Then from (31), we have

$$\frac{d\lambda}{d\tilde{t}} = \frac{1}{2}\tilde{v}\eta(\tilde{t}), \quad (35)$$

and (31) then implies

$$\xi(\tilde{t}) = \xi_{\text{in}} \exp\left(\frac{\tilde{v}}{2} \int_0^{\tilde{t}} \eta(\tilde{t}') d\tilde{t}'\right). \quad (36)$$

We now use (34) in (36) to estimate  $\xi(\tilde{t})$ :

$$\xi(\tilde{t}) = \frac{1}{2}\xi_{\text{in}}(2 + \tilde{v}\eta_{\text{in}}\tilde{t}). \quad (37)$$

Equations (34) (for  $\eta(\tilde{t})$  decreasing) and (37) (for  $\xi(\tilde{t})$  increasing) represent phase I of the transient, which (according to (32)), ends when the term  $(30 - 60s)\xi^2(\tilde{t})$  becomes comparable to  $\tilde{v}\eta^2/2$ . We now use these approximations to make an improved estimate of  $\eta(\tilde{t})$ , by substituting (37) into the RHS of (32):

$$\frac{d\eta}{d\tilde{t}} \approx -\frac{1}{2}\tilde{v}\eta(\tilde{t})^2 + (30 - 60s)\xi(\tilde{t})^2 \approx -\frac{2\tilde{v}\eta_{\text{in}}^2}{(2 + \tilde{v}\eta_{\text{in}}\tilde{t})^2} + \frac{1}{4}\xi_{\text{in}}^2(30 - 60s)(2 + \tilde{v}\eta_{\text{in}}\tilde{t})^2, \quad (38)$$

which we integrate to find an approximation for  $\eta$  down to its minimum:

$$\eta(\tilde{t}) \approx \frac{(1 - 2s)\xi_{\text{in}}^2[5\eta_{\text{in}}^3\tilde{v}^3\tilde{t}^4 + 40\eta_{\text{in}}^2\tilde{v}^2\tilde{t}^3 + 120\eta_{\text{in}}\tilde{v}\tilde{t}^2 + 120\tilde{t}] + 4\eta_{\text{in}}}{2(2 + \tilde{v}\eta_{\text{in}}\tilde{t})}. \quad (39)$$

Applying (36) with its improved approximation to  $\eta(\tilde{t})$  now gives

$$\xi(\tilde{t}) \approx \frac{1}{2}\xi_{\text{in}}(2 + \eta_{\text{in}}\tilde{v}\tilde{t}) \exp\left[-\frac{5}{16}(1 - 2s)\eta_{\text{in}}\tilde{t}^2\xi_{\text{in}}^2\tilde{v}(\eta_{\text{in}}\tilde{v}^2\tilde{t}^2 + 8\tilde{v}\tilde{t} + 24)\right]. \quad (40)$$

Equation (38) gives an approximation for the time to the minimum of  $\eta$  by setting the RHS to zero, that is

$$\frac{1}{2}\tilde{v}\left(\frac{2\eta_{\text{in}}}{2 + \tilde{v}\eta_{\text{in}}\tilde{t}}\right)^2 = \frac{1}{4}\xi_{\text{in}}^2(2 + \tilde{v}\eta_{\text{in}}\tilde{t})^2(30 - 60s), \quad (41)$$

which can be re-arranged as

$$T^4 = \frac{4\tilde{v}\eta_{\text{in}}^2}{15\xi_{\text{in}}^2(1 - 2s)}, \quad (42)$$

where  $T = 2 + \tilde{v}\eta_{\text{in}}\tilde{t}$ . Taking then the real positive root gives an estimate for  $\tilde{t}$ . We compared this estimate with numerical integration of equations (9), for three different values of  $\xi_{\text{in}}$  with  $s = 0.3904$ ,  $\tilde{v} = 0.1$ , and  $\eta_0 = 2.0713$ . The results are illustrated in Fig. 11.

When  $\xi_{\text{in}} = 0.000012094$  (which corresponds to steady motion with initial speed  $v_{\text{in}} = 0.000000001$ ), the theoretical minimum of  $\eta$  is 0.02260 at  $\tilde{t} = 1170$ , and the numerical integration gives  $\underline{\eta} = 0.0203$  at  $\tilde{t} = 1287$  (see figure 11(a)). When  $\xi_{\text{in}} = 0.0012094$  (corresponding to initial speed  $v_{\text{in}} = 0.00001$ ), the theory predicts a minimum of  $\underline{\eta} = 0.226$  at  $\tilde{t} = 108.3$ , and the numeric values are  $\underline{\eta} = 0.212$  at  $\tilde{t} = 116.9$  (see figure 11(b)). Finally, when  $\xi_{\text{in}} = 0.012094$  (corresponding to initial speed  $v_{\text{in}} = 0.001$ ), the theoretical minimum of  $\eta$  is 0.712 at  $\tilde{t} = 27.66$ , and the numeric values are  $\underline{\eta} = 0.716$  at  $\tilde{t} = 29.32$  (see figure 11(c)).

We can conclude that the theory gives reasonably accurate estimates. It is interesting to note that the values of  $\tilde{t}$  become large as  $\xi_{\text{in}}$  decreases. Consider what happens if we abruptly accelerate the slider from steady motion at speed  $v_{\text{in}}$  to final speed  $v$ . If  $v/v_{\text{in}}$  is close to unity, the results of section IV showed that the transient lasts for a time  $t_0 \sim L/v_{\text{in}}$ . If the ratio  $v/v_{\text{in}}$  is large, however, Eq. (42) implies that

$$\frac{\tilde{t}}{t_0} \sim \left(\frac{v}{v_{\text{in}}}\right)^{1/4}, \quad (43)$$

which is consistent with the results we have quoted for specific cases.

## B. Estimate of energy dissipated

Now we estimate the excess energy dissipated due to an abrupt acceleration. The dissipative force is given by equation (10), with the coefficients  $D_{ij}(\eta)$  specified in Appendix A. The force is greatest in the initial phase of the transient, when the gap parameter  $\xi$  is still very small. Accordingly, the force is dominated by the term containing the coefficient  $D_{11}$ :

$$F_x \sim -\frac{\tilde{v}\ln(1 + \eta(\tilde{t}))}{\xi(\tilde{t})\eta(\tilde{t})}. \quad (44)$$

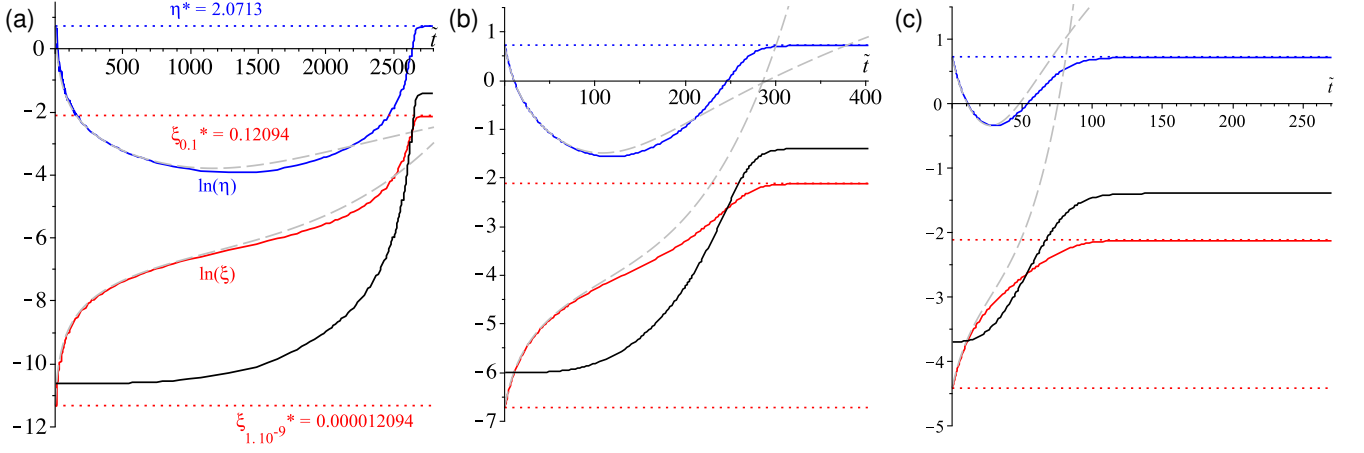


FIG. 11. Dynamics of a slider bearing pivoted at  $s = 0.3904$  with speed increasing instantaneously by three different factors: (a) a factor of  $10^8$ , from 0.000000001 to 0.1, (b) a factor of  $10^4$ , from 0.00001 to 0.1, and (c), a factor of  $10^2$  from 0.001 to 0.1. In all cases  $\eta$  (blue line) dips to a minimum then regains its equilibrium value,  $\xi$  (red line) increases to its new equilibrium value. The black line shows the bearing angle  $\theta$  and dashed grey lines are our approximations for  $\eta$  and  $\xi$  for phases I and II of the transient. Vertical scales are logarithmic.

Using equations (34) and (37), the dissipative force during phase I of the transient is

$$F_x(\tilde{t}) \sim -\frac{\tilde{v}}{\eta_{\text{in}}\xi_{\text{in}}} \ln\left(1 + \frac{2\eta_{\text{in}}}{2 + \tilde{v}\eta_{\text{in}}\tilde{t}}\right). \quad (45)$$

The energy dissipated up to time  $\tilde{t}$  is

$$E = \int_0^{\tilde{t}} d\tilde{t}' \tilde{v} F_x(\tilde{t}'). \quad (46)$$

Using equation (45) yields an analytic approximation:

$$\begin{aligned} E &= -\frac{\tilde{v}^2}{\eta_{\text{in}}\xi_{\text{in}}} \int_0^{\tilde{t}} d\tilde{t}' \ln\left(1 + \frac{2\eta_{\text{in}}}{2 + \tilde{v}\eta_{\text{in}}\tilde{t}'}\right) \\ &= -\frac{\tilde{v}}{\eta_{\text{in}}^2\xi_{\text{in}}} \left[ (\eta_{\text{in}}\tilde{t}\tilde{v} + 2\eta_{\text{in}} + 2) \ln\left(\frac{\eta_{\text{in}}\tilde{t}\tilde{v} + 2\eta_{\text{in}} + 2}{2 + \eta_{\text{in}}\tilde{t}\tilde{v}}\right) - 2\eta_{\text{in}} \ln\left(\frac{2\eta_{\text{in}} + 2}{2 + \eta_{\text{in}}\tilde{t}\tilde{v}}\right) - 2 \ln(\eta_{\text{in}} + 1) \right]. \end{aligned} \quad (47)$$

Figure 12 illustrates the dissipative force,  $F_x$ , and  $\eta$  during the transition from equilibrium at an initial constant speed to equilibrium at a much higher constant speed. This decreases very rapidly, indicating that the majority of energy dissipated in the transition occurs in the phase when  $\eta$  is decreasing to its minimum value.

We made a theoretical estimate of the total energy dissipated by evaluating (47) at the time  $\tilde{t}$ , estimated from equation (42). Figure 13 compares this estimate with the excess energy dissipation obtained from numerical integration. It illustrates both the increasing proportion of energy dissipated during speed transition as the speed increase factor grows (reaching 93% by a  $10^8$  times increase), and the close fit of our analytic model of energy dissipation to the minimum of  $\eta$  in comparison to the numeric model figures.

The foregoing shows that a vast majority of energy dissipated in achieving a very large bearing speed increase occurs in the period where  $\eta$  is decreasing to its minimum. We have a good analytic approximation for energy dissipated in this time interval and, using this to approximate the total energy dissipation, we are therefore able to look at the different energy dissipations for varying values of pivot position, our aim being to comment on whether the constant speed optimum,  $s = 0.3904$  remains a good choice in situations where frequent large speed variations will occur.

We might expect that, because moving the pivot point backwards increases the steady-state angle parameter  $\eta_0$ , this will reduce the drag experienced upon acceleration by facilitating entrainment of fluid under the bearing. The effects of changing the pivot point position were numerically significant, and consistent with this hypothesis, but not especially dramatic. We investigated speed increases by factors of  $10^8$ ,  $10^2$ , and 10 times up to a final speed  $\tilde{v} = 0.1$ . The excess energy dissipation values are plotted in Fig. 14, illustrating the reduced energy dissipation during the

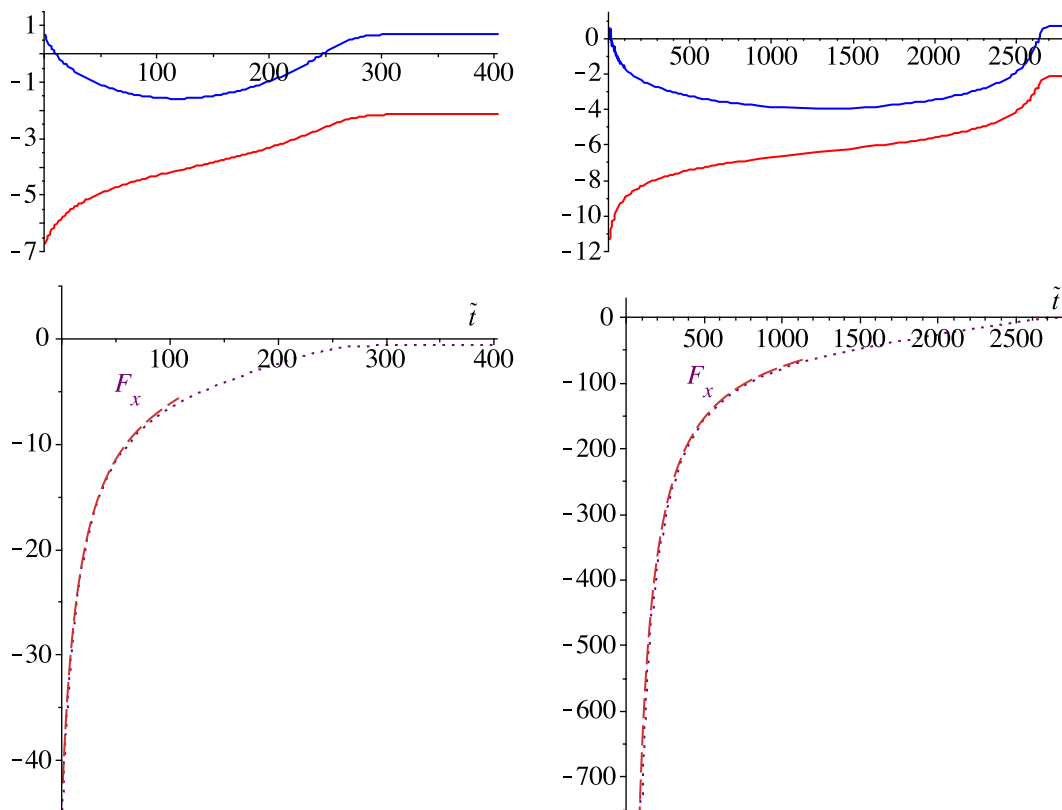


FIG. 12. Lower panels show that the dissipative force (purple dot is numerical result, orange dash is analytic approximation) is most significant, well approximated by (45), during phase I of the motion. Left side plots show a  $10^4$  times speed increase, right hand plots show a  $10^8$  times speed increase. The upper plots show  $\eta$  (blue) and  $\xi$  (red), both log scale, with  $\eta$  dipping to a minimum and regaining equilibrium, in order to make a comparison with the phases of the motion defined by figure 10. In both cases  $s = 0.3904$ ,  $\tilde{v} = 0.1$ .

transient when the pivot point is moved closer to the trailing edge. The improvement is of the order of 60%, 55% and 50% energy saving when moving  $s$  from 0.3904 to 0.3 at speed increase factors of  $10^8$ ,  $10^2$ , and 10 respectively. However, changing the pivot point causes a large increase of the dissipation rate for a bearing moving at constant speed (see Fig. (3)), so that the speed fluctuations would have to occur very frequently in order for these improvements in transient response to become significant.

## VII. CONCLUDING REMARKS

We have obtained the full equations of motion for pivoted slider bearings. Our primary motivation was to investigate the transient motion of the slider after an abrupt increase in its velocity. Our numerical results show that this is quite complex, as illustrated in Figs. 10-11. We were able to analyse this complex transient, and to make an analytical approximation for the time-dependence of the dynamical variables during its crucial initial stages. We were also able to quantify the additional energy dissipation which occurs when the speed of the slider bearing is abruptly increased.

In order to obtain the equations of motion, we introduced a general notion of a *transversion* procedure, to change the dependent variables in a dynamical process with linear equations of motion. Using this approach we were able to obtain the equations of motion from those of a sinking plate, which were obtained in [5].

We also determined the sinking motion of the slider after sliding motion ceases, and showed that the steady-state solutions investigated in [4] are, in fact, stable.

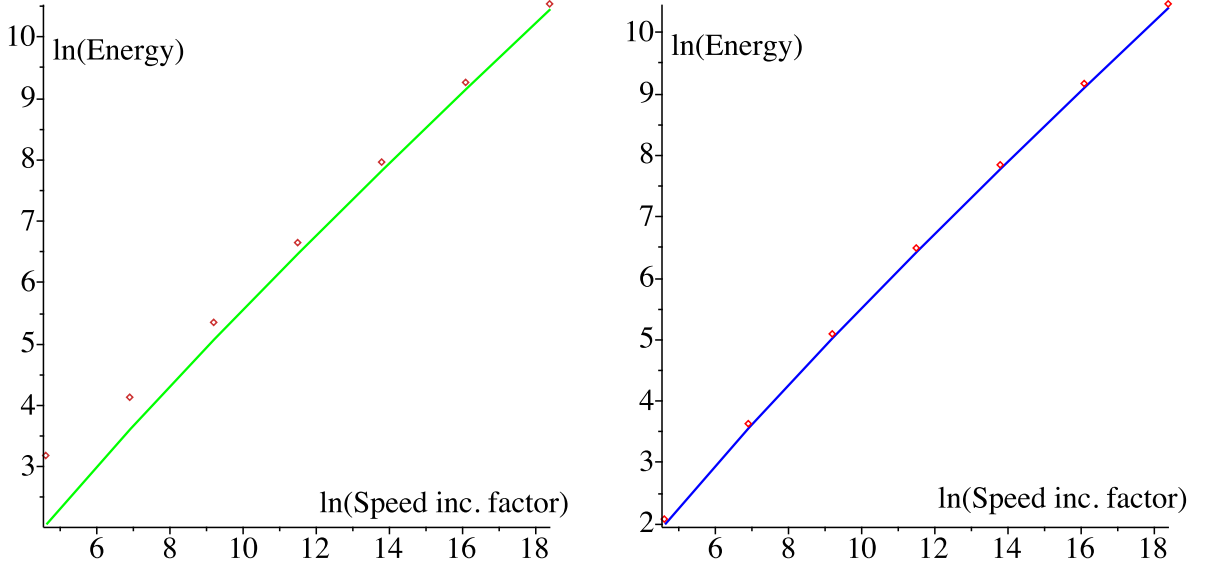


FIG. 13. Plots of excess energy dissipated after an abrupt speed increase. The left pane shows the total energy dissipated at speed increase factors  $10^i$ ,  $i = 2$  to  $8$  (orange diamonds) and the energy dissipated to the minimum of  $\eta$  (green line), both from the numeric model. The right pane shows energy dissipated to the minimum of  $\eta$  as given by the numeric model at the same speed increase factors (red diamonds) and the energy dissipated as predicted by the analytic model (blue line). In both cases  $s = 0.3904$ ,  $\tilde{v} = 0.1$ .

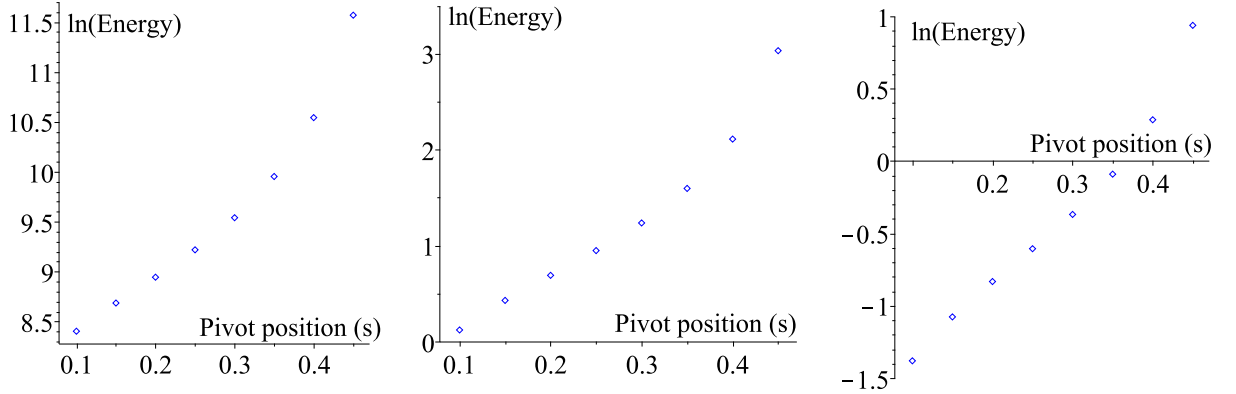


FIG. 14. Plot of energy dissipated during equilibrium transition through to the minimum of  $\eta$ , as a function of the pivot position  $s$ , following an abrupt speed change. Left, middle and right panels show speed increases of  $10^8$ ,  $10^2$ , and  $10$  times, respectively.  $\tilde{v} = 0.1$  is used throughout.

#### ACKNOWLEDGMENTS

We thank Prof. G. W. Milton for pointing out the relevance of the Schur complement to equation (7).

- 
- [1] BATCHELOR, G. K. 1967 An Introduction to Fluid Dynamics. Cambridge University Press, ISBN 978-0-521-66396-0.  
[2] SZERI, A.S. 1998 Fluid Film Lubrication. Cambridge University Press, ISBN 978-0-521-89823-2.  
[3] ORON, A., DAVIS, S. H., BANKOFF, S. G. 1997 Long-scale evolution of thin liquid films, *Rev. Mod. Phys.*, **69**, 931.  
[4] MICHELL, A.G.M. 1950 Lubrication, its Principles and Practice. Blackie.  
[5] WILKINSON, A., PRADAS, M. AND WILKINSON, M. 2023 Lubrication dynamics of a settling plate, *J. Fluid Mech.*, in press, arXiv:2303.13678.



- [6] REYNOLDS, O. 1886 On the Theory of Lubrication and Its Application to Mr. Beauchamp Tower's Experiments, Including an Experimental Determination of the Viscosity of Olive Oil. *Phil. Trans. Roy. Soc. Lond.* **11**, pp. 157-234, <http://dx.doi.org/10.1098/rstl.1886.0005>.
- [7] HAPPEL, J. AND BRENNER, H. 1983 Low Reynolds Number Hydrodynamics. Martinus Nijhof, Hague, ISBN-13: 978-90-247-2877-0.
- [8] ZHANG, F. (ED.) 2005 The Schur Complement and Its Applications, Numerical Methods and Algorithms. Vol. 4. Springer, ISBN 0-387-24271-6. doi:10.1007/b105056.

#### APPENDIX A: MATRIX COEFFICIENTS

We list the matrix elements of  $\mathbf{B}$ , defined by equation (5). In the following expressions,

$$\psi = \ln(\eta + 1) . \quad (48)$$

The elements are:

$$\begin{aligned}
 B_{11} &= \frac{(-4\eta - 8)\psi + 6\eta}{(\eta + 2)\eta} \\
 B_{12} &= \frac{(-6\eta - 6)\psi + 3\eta^2 + 6\eta}{(\eta + 2)\eta^2} \\
 B_{13} &= \frac{(-12\eta - 18)\psi + 3\eta^2 + 18\eta}{(\eta + 2)\eta^3} \\
 B_{21} &= \frac{(6\eta + 12)\psi - 12\eta}{(\eta + 2)\eta^2} \\
 B_{22} &= \frac{(12\eta + 12)\psi - 6\eta^2 - 12\eta}{(\eta + 2)\eta^3} \\
 B_{23} &= \frac{(24\eta + 36)\psi - 6\eta^2 - 36\eta}{(\eta + 2)\eta^4} \\
 B_{31} &= \frac{(-12\eta - 18)\psi + 3\eta^2 + 18\eta}{(\eta + 2)\eta^3} \\
 B_{32} &= -\frac{3}{2} \frac{((2\eta + 2)\psi + \eta^2 - 2\eta)((-2\eta - 2)\psi + \eta^2 + 2\eta)}{(\eta + 2)\eta^5} \\
 B_{33} &= \frac{12(\eta + 1)^2\psi^2 + (-72\eta^2 - 96\eta)\psi - 3\eta^2(\eta^2 - 4\eta - 28)}{2(\eta + 2)\eta^6} \quad (49)
 \end{aligned}$$

The matrix elements of  $\mathbf{C} = \mathbf{B}^{-1}$  are:

$$\begin{aligned}
C_{11} &= -\frac{\eta}{\psi} \\
C_{12} &= \frac{-\eta^2}{2\psi} \\
C_{13} &= 0 \\
C_{21} &= \frac{-\eta^2}{2\psi} \\
C_{22} &= \frac{(4(\eta+1)^2\psi^3 - (6\eta^2+8\eta)\psi^2 - \eta^2(\eta^2+8\eta+2)\psi + 3\eta^4 + 6\eta^3)\eta^3}{3((-2\eta-2)\psi + \eta^2 + 2\eta)\psi((2\eta+2)\psi^2 + (\eta^2+2\eta)\psi - 4\eta^2)} \\
C_{23} &= \frac{((-4\eta-6)\psi + \eta^2 + 6\eta)\eta^5}{3((-2\eta-2)\psi + \eta^2 + 2\eta)((2\eta+2)\psi^2 + (\eta^2+2\eta)\psi - 4\eta^2)} \\
C_{31} &= \frac{\eta^3}{2\psi} \\
C_{32} &= \frac{((2\eta+2)\psi^2 + (\eta^2+\eta)\psi - 3\eta^2)\eta^4}{3\psi((2\eta+2)\psi^2 + (\eta^2+2\eta)\psi - 4\eta^2)} \\
C_{33} &= -\frac{\eta^6}{(6\eta+6)\psi^2 + (3\eta^2+6\eta)\psi - 12\eta^2}
\end{aligned} \tag{50}$$

The matrix elements  $D_{ij}(\eta)$  are:

$$\begin{aligned}
D_{11}(\eta) &= -\frac{\psi}{\eta} \\
D_{12}(\eta) &= -\frac{\eta}{2} \\
D_{13}(\eta) &= 0 \\
D_{21}(\eta) &= \frac{\eta}{2} \\
D_{22}(\eta) &= -\frac{(4\psi^2\eta^2 - \eta^4 + 8\psi^2\eta - 24\psi\eta^2 + 4\eta^3 + 4\psi^2 - 32\psi\eta + 28\eta^2)\eta^3}{12(4\psi^3\eta^2 - \psi\eta^4 + 8\psi^3\eta - 12\psi\eta^3 + 4\eta^4 + 4\psi^3 - 12\psi\eta^2 + 8\eta^3)} \\
D_{23}(\eta) &= \frac{(4\psi\eta - \eta^2 + 6\psi - 6\eta)\eta^5}{3(4\psi^3\eta^2 - \psi\eta^4 + 8\psi^3\eta - 12\psi\eta^3 + 4\eta^4 + 4\psi^3 - 12\psi\eta^2 + 8\eta^3)} \\
D_{31}(\eta) &= -\frac{\eta^2}{2} \\
D_{32}(\eta) &= \frac{\eta^4(2\psi\eta + \eta^2 + 2\psi - 2\eta)}{12(2\psi^2\eta + \psi\eta^2 + 2\psi^2 + 2\psi\eta - 4\eta^2)} \\
D_{33}(\eta) &= -\frac{\eta^6}{3(2\psi^2\eta + \psi\eta^2 + 2\psi^2 + 2\psi\eta - 4\eta^2)}
\end{aligned} \tag{51}$$